# Dynamics at an exceptional point in an interacting quantum dot system

**William Samuelson**


LUND
UNIVERSITY

A Bachelor Thesis at the Division of
Solid State Physics

Supervised by Martin Leijnse and Stephanie Matern

Lund University
August 26, 2022

# Dynamics at an exceptional point in an interacting quantum dot system

**William Samuelson**

## Abstract

Lorem ipsum dolor sit amet, consectetuer adipiscing elit. Ut purus elit, vestibulum ut, placerat ac, adipiscing vitae, felis. Curabitur dictum gravida mauris. Nam arcu libero, nonummy eget, consectetuer id, vulputate a, magna. Donec vehicula augue eu neque. Pellentesque habitant morbi tristique senectus et netus et malesuada fames ac turpis egestas. Mauris ut leo. Cras viverra metus rhoncus sem. Nulla et lectus vestibulum urna fringilla ultrices. Phasellus eu tellus sit amet tortor gravida placerat. Integer sapien est, iaculis in, pretium quis, viverra ac, nunc. Praesent eget sem vel leo ultrices bibendum. Aenean faucibus. Morbi dolor nulla, malesuada eu, pulvinar at, mollis ac, nulla. Curabitur auctor semper nulla. Donec varius orci eget risus. Duis nibh mi, congue eu, accumsan eleifend, sagittis quis, diam. Duis eget orci sit amet orci dignissim rutrum.

# Contents

# Chapter 1

# Introduction

The theory of quantum mechanics developed in the last century has been proved to be extremely successful in describing nature at the small scale. Typical systems treated by standard quantum mechanics are nuclei, atoms, and other systems which can be assumed to be isolated from the environment. In such systems, the Hamiltonian is postulated to be Hermitian, guaranteeing that energies are real-valued and that probabilities are conserved throughout the evolution of the system. However, in many systems, there is significant dissipation into and out of the system, and hence cannot accurately be described by standard quantum mechanics (what systems?). One way to handle such open systems is to loosen the requirement of the Hermiticity of the Hamiltonian. The resulting field of non-Hermitian quantum physics has successfully been describing systems in nuclear, atomic and optical physics in recent decades [1]. One property of particular interest in non-Hermitian operators is the possibility of exceptional points (EPs). These correspond to points in parameter space where two or more eigenvalues and their corresponding eigenvectors of the operator simultaneously coalesce. Exceptional points have been proposed to have several useful technological applications, and along with the optical microring experiments in 2017, exceptional point sensors successfully increased the sensitivity of current and nano-particle detection [2, 3].

A different framework which treats open systems is quantum master equations, where the dynamics of the system is captured by the Liouvillian superoperator. Similarly to the Hamiltonian in non-Hermitian physics, the Liouvillian is not Hermitian due to the coupling to the environment. This brings the possibility of exceptional points also in the Liouvillian superoperator. EPs in Liouvillian physics have been of particular theoretical interest recently, and is proposed to have important applications in control and sensing technologies. Two recent examples include Ref. [4], where critical decay towards the steady state in a quantum thermal machine was found at the EP; and in Ref. [5] where an EP corresponded to optimal steering toward a target quantum state.

An application of particular interest for quantum master equations and Liouvillian physics is electron transport in systems of quantum dots connected to metallic leads [6]. A quantum dot is a fabricated semiconductor structure containing a small number of electrons and is typically in the order of 100 nanometres in size [7]. The size of the dot needs to be small in comparison with the thermal wavelength of the electrons, which is why experiments are generally realized at temperatures close to absolute zero [8]. One method of creating this tiny isolation of electrons is to

apply voltages via nanoscale electrodes, called gates, which depletes the number of electrons in a small region, see Fig. 1.1a. If the voltages are tuned successfully, the quantum dot can be tunnel coupled to the two surrounding conducting regions of the semiconductor, known as the source and drain. The electrons can then tunnel from the source into the dot and then exiting it by tunneling into the drain, producing a current through the system [7]. This process is schematically presented in Fig. 1.1b.

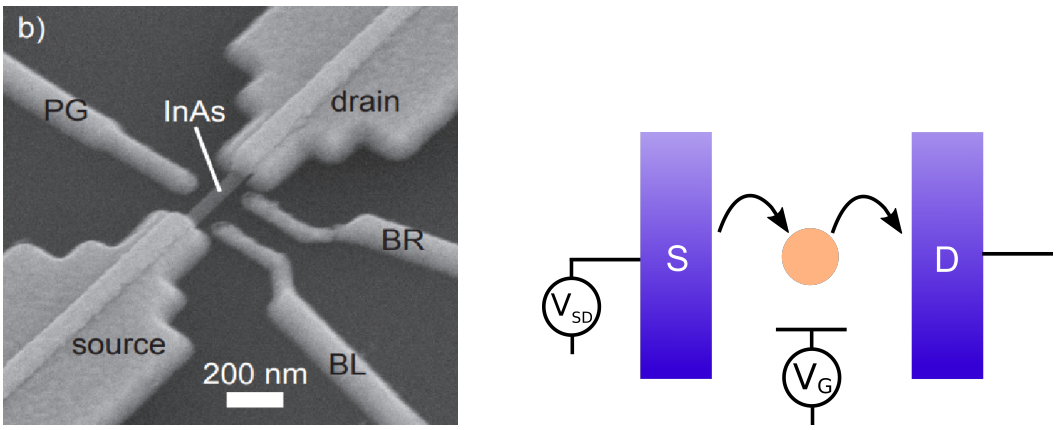


(a) (b)

Figure 1.1: a) A physical implementation of a single quantum dot system. The quantum dot, labeled with InAs, the source and drain, and the gates (BR, BL and PG) are all clearly visible in this figure, captured by a scanning tunneling microscope. The figure is taken from Ref. [9]. b) A schematic figure of a quantum dot system where the quantum dot is in the center, tunnel coupled to the source (S) and drain (D). The gate voltage $V_G$ and the source-drain voltage $V_{SD}$, are tuned to define the quantum dot.

The wide tunability of the optical, electrical and chemical properties of quantum dots has made them useful in a large span of applications. These range from energy harvesting, display technologies, and sensors to medical and biological applications (Source). The transport set-up given in Fig. 1.1 in particular, has been used as a single-electron transistor

Write about QD transport and why it is interesting. Sensing. However, exceptional point physics in QDs has not been investigated very much. In this thesis, we study a quantum dot system consisting of two quantum dots coupled in parallel to metallic leads. 2nd order EP.

In this thesis, we study non-equilibrium transport properties of a parallel quantum dot system, with focus on the transient current. In particular, the dynamics at a second order EP is evaluated and understood using a combination of numerical and analytical approaches. Inspired by Ref. [4] and its study of EPs in thermal machines, the main purpose of the thesis is to see if similar results are visible in quantum dot systems.

The thesis is divided in the following chapters: in

# Chapter 2

# Theory

The theory chapter of the thesis is divided into three sections. Firstly, a brief overview of the theory behind transport through quantum dots is given. Then, the focus is turned to some of the tools used in open quantum systems, ultimately ending in a section about quantum master equations. The final section will further explain the notion of exceptional points, and introduce a couple of important tools used in exceptional point physics. Throughout the following parts of the thesis, we will set $\hbar = 1$, $k_b = 1$, and $|e| = 1$.

## 2.1 Transport through quantum dots

To begin understanding the transport of electrons through a system of quantum dots, it is insightful to first study the single quantum dot system. The following explanation is inspired by reference [8].

Consider a single quantum dot with $N$ electrons capacitively coupled to a gate and coupled to source and drain reservoirs through tunnel junctions as in Fig. 1.1b. The main transport properties of the system can then be understood in terms of the chemical potentials of the quantum dot and the source and drain reservoirs. These are often depicted in electro-chemical potential diagrams, see Fig. 2.1. There, $\mu(N)$ is the energy required to add the $N$th electron to the quantum dot, and $\mu_S$ and $\mu_D$ are the Fermi levels of the source and drain. The shaded areas represent the Fermi-Dirac distributions of the reservoirs.

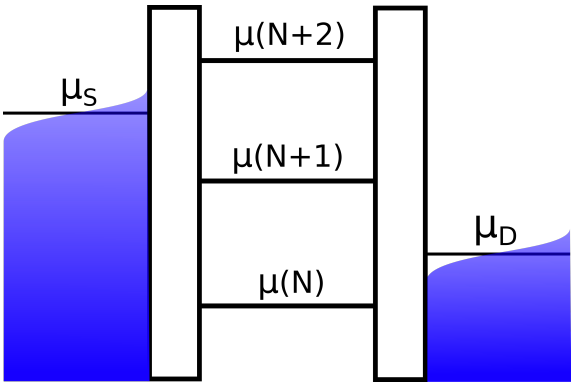


Figure 2.1: An electro-chemical potential diagram of the single quantum dot system. The source and drain are in a thermal distribution given by the shaded areas with Fermi levels $\mu_S$ and $\mu_D$. The quantum dot is depicted as a ladder with energies $\mu(N)$, representing the energy required to add the $N$th electron to the dot.

Using this picture, the electron transport through the quantum dot can be easily visualized. If the chemical potential levels are located as in Fig. 2.1, $\mu(N+1)$ is below $\mu_S$, and an electron will likely tunnel from the source onto the dot, increasing the number of electrons on the dot from $N$ to $N+1$. After the tunneling event, there is an even lower chemical potential available for the electron, $\mu_D$, and the electron will with a high probability leave the quantum dot and enter the drain. In this fashion, the system will cycle through having $N$ and $N+1$ electrons on the dot, producing a current.

It turns out that $\mu(N)$ depends linearly on the gate voltage $V_G$, so by changing it, the ladder of states in Fig. 2.1 can be lowered or raised. The source-drain voltage $V_{SD}$ on the other hand, changes the distance between $\mu_S$ and $\mu_D$. Through these two processes, it is possible to change the electro-chemical potential landscape and therefore control the current through the system. This captures the main behavior of the dynamics of the quantum dot system. However, by adapting the theory of open quantum systems, a much richer and more accurate theory can be developed.

## 2.2 The theory of open quantum systems

Open quantum systems are systems which are non-isolated and connected to some sort of environment. Often, it considers a total system consisting of the (sub)system of interest, and an environment. The total system is closed, and therefore it obeys the standard quantum mechanical equations of motion. The goal of the theory of open quantum systems is to infer the dynamics of the smaller system from the equations of the total system [10]. To do this, a few fundamental tools used in this field need to be introduced.

### 2.2.1 The von Neumann equation and the reduced density operator

An essential tool used in the theory of open quantum systems is the density operator $\hat{\rho}$. In such systems, the exact state of the system is generally unknown. Instead, the system may be known to be in a state $|\psi_k\rangle$ with a probability $p_k$, or in another state

$|\psi_l\rangle$ with a different probability $p_l$. Generally, the system is then said to be in an ensemble $\{|\psi_k\rangle, p_k\}_k$. The density operator describes this information in a compact way:

$$\hat{\rho} = \sum_k p_k |\psi_k\rangle \langle\psi_k| . \tag{2.1}$$

It can easily be shown that the density operator is Hermitian and has unity trace. Furthermore, by fixing a basis $\{|\phi_i\rangle\}$, the density operator can be represented by its matrix elements

$$\rho_{ij} = \langle\phi_i|\hat{\rho}|\phi_j\rangle = \sum_k p_k \langle\phi_i|\psi_k\rangle \langle\psi_k|\phi_j\rangle . \tag{2.2}$$

The diagonal elements $\rho_{ii}$ represents classical probabilities of being in a state $|\phi_i\rangle$ and the off-diagonal elements $\rho_{ij}$ are the so called coherences between state $|\phi_i\rangle$ and $|\phi_j\rangle$. Note that the matrix elements are basis dependent, and that there always is a basis in which the density operator is diagonal [11].

The average measured value of an observable $\hat{O}$ of an ensemble represented by $\hat{\rho}$ is given by

$$\langle\hat{O}\rangle = \mathrm{Tr}(\hat{\rho}\hat{O}). \tag{2.3}$$

From the density operator one can therefore extract all signifiant information from the ensemble, and it can be described as the "state" of the system. It is also possible to calculate how the density operator evolves over time. Under a Hamiltonian $\hat{H}$, the evolution is given by the von Neumann equation

$$\frac{\mathrm{d}\hat{\rho}}{\mathrm{d}t} = i[\hat{\rho}, \hat{H}] \equiv \mathcal{L}\hat{\rho}, \tag{2.4}$$

where $\mathcal{L}$ is the Liouvillian superoperator, or just the Liouvillian [11].

The Liouvillian $\mathcal{L}$ in Eq. (2.4) is an operator acting on an operator, hence being called a superoperator. However, it is possible to treat it as a normal operator which acts on a Hilbert space spanned by the density matrices. The Liouvillian can therefore be represented by a matrix $L$, which acts on a vector representation of the density matrices, usually written as $|\rho\rangle\rangle$. The Hilbert space spanned by these vectors is called the Fock-Liouville space, equipped with a scalar product $\langle\langle\rho_1|\rho_2\rangle\rangle$ [10].

Returning to the mentioned goal of the theory of open quantum systems, a natural question is the following:How do we extract the density operator of a subsystem $\hat{\rho}_S$, from the total density operator $\hat{\rho}_T$, the latter describing the closed, full system? This question is resolved by the reduced density operator. If the total system $T$ consists of a subsystem $S$ and an environment $E$, then the reduced density matrix for the subsystem is given by

$$\hat{\rho}_S = \mathrm{Tr}_E(\hat{\rho}_T), \tag{2.5}$$

where $\mathrm{Tr}_E$ is the partial trace over the environment. The partial trace essentially takes the average with respect to the environmental degrees of freedom. This way, a density operator for the subsystem of interest is obtained without having to simulate the whole system. The reduced density operator contains all measurement statistics of interest in the subsystem, placing it at the core of the theory of open quantum systems [11].

### 2.2.2 The Lindblad Master equation

An important framework for determining the dynamics of an open quantum system is the master equation approach. A classical master equation is defined by

$$\frac{\mathrm{d}p_i}{\mathrm{d}t} = \sum_j R_{ji}p_j - \sum_j R_{ij}p_i, \tag{2.6}$$

with probabilities $p_i$ of being in state $|\psi_i\rangle$, and transition rates $R_{ij}$ describing the rate of transitions from $|\psi_i\rangle$ to $|\psi_j\rangle$. As an example, the states in a quantum dot system may correspond to the number of electrons on the dot while the transition rates are typically related to the Fermi-Dirac distributions of the reservoirs and the tunneling rates of the barriers [8].

Collecting the rate equations for each $i$ and adding the condition $\sum_i p_i = 1$ such that the total probability is unity, a system of ordinary differential equations is obtained. This can be solved numerically using standard methods for first order differential equations, such as the Runge-Kutta method [12]. Once the probabilities $p_i(t)$ are obtained, the evolution of the system can be calculated. Returning to the quantum dot example, the transient dynamics of the current can then be calculated by considering the amount of charge tunneling through the barriers at each point in time, which is directly related to the tunneling rates and probabilities $p_i(t)$ [8].

While a classical master equation may give accurate results for some quantum systems, it leaves out important physics. A quantum master equation generalizes the notion of a classical master equation in the following sense: The unknown in a quantum master equation does not only contain the probabilities $p_i$ of being in a quantum state $|\psi_i\rangle$, but also the coherences. Hence, a quantum master equation involves the full density matrix while a classical master equation only includes the diagonal elements. However, since it always is possible to find a basis such that the density matrix is diagonal, the two master equations can be equivalent in certain bases.

The starting point for quantum master equations is Eq. (2.4), the von Neumann equation, for the density matrix of the total system. Using the partial trace, a differential equation for the reduced density matrix of the system of interest (from now on written as $\hat{\rho}$) can be obtained. However, the resulting equation still includes the total density operator and approximations have to be made [10]. One common approximation is to assume that the coupling between the system and the environment is weak in comparison to the other energy scales of the system. This way, the interaction can be treated perturbatively. One of the most established quantum master equations, the Lindblad equation, is derived in this fashion [13], and is given by

$$\frac{\mathrm{d}\hat{\rho}}{\mathrm{d}t} = i[\hat{\rho}, \hat{H}_{\mathrm{eff}}] + \sum_i \hat{L}_i\hat{\rho}\hat{L}_i^\dagger - \frac{1}{2}\hat{\rho}\hat{L}_i^\dagger\hat{L}_i - \frac{1}{2}\hat{L}_i^\dagger\hat{L}_i\hat{\rho} \equiv \mathcal{L}\hat{\rho}, \tag{2.7}$$

where $\hat{H}_{\mathrm{eff}}$ is the sum of two terms: the subsystem Hamiltonian $\hat{H}_{\mathrm{S}}$ and the Lamb shift Hamiltonian $\hat{H}_{\mathrm{LS}}$, a renormalization of energy levels due to the interaction with the environment [10]. The operators $\hat{L}_i$ are the so called jump operators, which capture the coupling processes to the environment. In Ref. [14], a phenomenological approach for calculating the jump operators is described. Using this so called PER-Lind approach, each jump operator is associated with an actual, physical process. Taking a quantum dot system as an example, every jump operator then represents

a certain tunneling event. Once the jump operators are constructed and the first term of Eq. (2.7) is calculated, an expression for the Liouvillian $\mathcal{L}$ can be obtained.

The right hand side of the Lindblad equation can be divided into two parts. The first term, $i[\hat{\rho}, \hat{H}_{\text{eff}}]$, describes the unitary, free evolution of the system. A simple example of a free evolution would be the precession of magnetic moment in a magnetic field. The sum over $i$ on the other hand, correspond to the non-unitary and dissipative part of the dynamics [11]. The latter part causes the total Liouvillian to be non-Hermitian, which brings the possibility of exceptional points in the matrix representation of the Liouvillian.

## 2.3 Exceptional points

A matrix which describes the evolution of a physical system, such as a Hamiltonian or a Liouvillian matrix, generally depends on the parameters of the system. These parameters span the so called parameter space, and it is in this space the exceptional points lie. An exceptional point is defined as a point in the parameter space which causes two or more eigenvalues and their eigenvectors to simultaneously coalesce [1]. An EP is said to be of a certain order, reflecting how many eigenvectors coalesce at the point. The notion of exceptional points and its orders are directly related to a type of matrix decomposition, the Jordan normal form.

### 2.3.1 Jordan normal form

In physics, a common way to simplify calculations is to diagonalize the matrix generating the evolution of the system. The diagonalization process can be understood a change of basis to linearly independent eigenvectors, obeying $Ar_i = \lambda_i r_i$ [15]. In this basis, the linear transformation of the matrix is very simple: it scales each eigenvector $r_i$ by the corresponding eigenvalue $\lambda_i$. The matrix in the new basis is therefore diagonal, explaining the name of the process. For a matrix $A$ and its diagonal form $D$, this can be written as

$$A = SDS^{-1}, \tag{2.8}$$

where $S = (r_1, \ldots, r_n)$ consists of the eigenvectors of $A$.

However, not all matrices can be diagonalized, the exceptions being called defective matrices. For a defective matrix, there does not exist a basis of eigenvectors, and the diagonalization process is not possible [15]. This is closely related to the notion of exceptional points, since when two eigenvectors coalesce, one dimension is lost and the eigenvectors do not form a basis anymore. A matrix at an EP is therefore always defective.

Fortunately, there is a notion of an "almost diagonal" form for defective matrices, called the Jordan normal form. Recall that in the diagonalizable case, the basis is changed to the linearly independent eigenvectors. To construct the Jordan form for a defective matrix, this basis has to be completed in some way to span the full space. This can be done using Jordan chains [15], which for each eigenvector $r_i$ with

eigenvalue $\lambda_i$, consist of vectors $r_i, r_i^{(2)}, \ldots, r_i^{(n_i)}$ defined by

$$\begin{aligned}(A-\lambda_i I)r_i &= 0,\\ (A-\lambda_i I)r_i^{(2)} &= r_i,\\ (A-\lambda_i I)r_i^{(3)} &= r_i^{(2)},\\ &\vdots\\ (A-\lambda_i I)r_i^{(n_i)} &= r_i^{(n_i-1)},\end{aligned} \tag{2.9}$$

where $I$ is the identity matrix. The length of the $i$th chain, $n_i$, depends the number of coalescing eigenvectors, and is therefore the same as the order of the corresponding EP. Note that for eigenvectors not involved in an EP, i.e., for eigenvectors which have not coalesced, the Jordan chain is of length one, only consisting of the eigenvectors themselves.

The vectors forming the Jordan chain are also known as the right generalized eigenvectors, which indicates the notion of *left* generalized eigenvectors. Regular left eigenvectors $l_i$ are row vectors, defined by $l_i A = \lambda_i A$. These can then be extended to left generalized eigenvectors in a similar way as the right ones, forming Jordan chains $l_i, l_i^{(2)}, \ldots, l_i^{(n_i)}$. The left generalized eigenvectors can be constructed such that $l_i^{(s)} r_j^{(t)} = \delta_{ij}\delta_{st}$, i.e, biorthogonally to the right generalized eigenvectors [1]. Creating these left and right Jordan chains for each linearly independent eigenvector results in $q$ pairs of chains, each of which are collected into the matrices

$$\begin{aligned}&\{\boldsymbol{r}_i\}_{i=1}^{q}, \text{ where } \boldsymbol{r}_i = \begin{bmatrix} r_i & r_i^{(2)} & \ldots & r_i^{(n_i)} \end{bmatrix},\\ &\{\boldsymbol{l}_i\}_{i=1}^{q}, \text{ where } \boldsymbol{l}_i = \begin{bmatrix} l_i \\ l_i^{(2)} \\ \ldots \\ l_i^{(n_i)} \end{bmatrix}\end{aligned} \tag{2.10}$$

Here, the bold font in $\boldsymbol{r}_i$ ($\boldsymbol{l}_i$) indicates a collection of column (row) vectors next to (below) each other, forming a matrix. The set of right generalized eigenvectors from all Jordan chains is called the canonical basis of the transformation. Using this new basis, the transformation matrix $M$ can be formed:

$$M = \begin{bmatrix} \boldsymbol{r}_1 \ldots \boldsymbol{r}_q \end{bmatrix}, \tag{2.11}$$

which also is known as the modal matrix. The inverse modal matrix $M^{-1}$, can be formed in terms of the left generalized eigenvectors:

$$M^{-1} = \begin{bmatrix} \boldsymbol{l}_1 \\ \vdots \\ \boldsymbol{l}_q \end{bmatrix}, \tag{2.12}$$

since $\boldsymbol{l}_j \boldsymbol{r}_i = \delta_{ij} I$ where $I$ is the $n_j \times n_i$ identity matrix. This follows from the biorthogonality of the left and right generalized eigenvectors.

The Jordan normal form of $A$ is then finally obtained by forming $J = M^{-1}AM$

and has the following structure:

$$J = \begin{bmatrix} J_{n_1}(\lambda_1) & \dots & 0 \\ \vdots & \ddots & \vdots \\ 0 & \dots & J_{n_q}(\lambda_q) \end{bmatrix}, \text{ where } J_{n_i}(\lambda_i) = \begin{bmatrix} \lambda_i & 1 & \dots & 0 \\ \vdots & \ddots & \ddots & \vdots \\ \vdots & & \ddots & 1 \\ 0 & \dots & \dots & \lambda_i \end{bmatrix}. \tag{2.13}$$

The Jordan form hence consists of $q$ Jordan blocks $J_{n_i}(\lambda_i)$ on the diagonal, where each block is of size $n_i$ and consists of its eigenvalue on the diagonal and ones on the super diagonal [15]. Note that if all blocks are of size one, i.e., there are no exceptional points, the Jordan form is diagonal. The Jordan normal form can therefore be thought of a generalization of the diagonal form $D$.

Unfortunately, the Jordan form of a matrix is notoriously difficult to calculate numerically. This stems from the fact that an arbitrary small perturbation away from an EP completely changes the Jordan form. The process is therefore inherently numerically unstable [16]. For simple cases, it is however possible to work around this difficulty by introducing a small tolerance to determine if eigenvalues and their eigenvectors have coalesced. One can then infer the block structure of the Jordan form and construct it manually.

To be able to use the Jordan form in calculations, a substitution $A \to MJM^{-1}$ has to be made, and hence, the matrices $M$ and $M^{-1}$ are also desirable to compute numerically. These matrices consist of the right and left generalized eigenvectors, which can be calculated by the following process. Firstly, the regular eigenvectors are calculated by some numerical method, e.g., the `scipy.linalg.eig` function in Python. If there are coalesced eigenvectors (within the tolerance), the corresponding Jordan chains need then to be computed. This can be done by solving the defining equations for the generalized eigenvectors given by Eq. (2.9). However, since $A-\lambda_i I$ is not of full rank, the equations are underdetermined, meaning that there does not exist a unique solution. A standard way of solving this problem is by using the Moore-Penrose pseudoinverse, which finds one of the solutions to the equation [15]. This process is then repeated until the full Jordan chains for each set of coalescing eigenvectors are calculated, obtaining all of the generalized eigenvectors. Finally, by biorthogonalizing the two set of vectors, the modal matrix $M$ and its inverse $M^{-1}$ are obtained. Alternatively, $M^{-1}$ can be calculated by numerically inverting $M$.

### 2.3.2 General solution of ODEs

A useful application of the Jordan form is for analytical solutions of ordinary differential equations (ODEs). An ODE is a linear differential equation of the form

$$\frac{\mathrm{d}x}{\mathrm{d}t} = Ax. \tag{2.14}$$

Often, the unknown $x$ is a vector, and $A$ a matrix. The solution can then be written as a matrix exponential in the following way:

$$x(t) = e^{At}x(0), \text{ where } e^{At} = \sum_{k=0}^{\infty} \frac{(At)^k}{k!}. \tag{2.15}$$

The matrix exponential can be simplified using Jordan decomposition. It can be shown that $e^{At} = Me^{Jt}M^{-1}$ where $M$ is the modal matrix and

$$e^{Jt} = \begin{bmatrix} e^{J_{n_1}(\lambda_1)t} & \dots & 0 \\ \vdots & \ddots & \vdots \\ 0 & \dots & e^{J_{n_q}(\lambda_q)t} \end{bmatrix}, \text{ where } e^{J_{n_i}(\lambda_i)t} = e^{\lambda_i t} \begin{bmatrix} 1 & t & \dots & \frac{t^{n_i-1}}{(n_i-1)!} \\ \vdots & \ddots & \ddots & \vdots \\ \vdots & & \ddots & t \\ 0 & \dots & \dots & 1 \end{bmatrix}. \tag{2.16}$$

The matrix exponential therefore consists of entries with terms of the form $t^k e^{\lambda_i t}$ [15]. Note that if $A$ is diagonalizable, all blocks are of size one and the entries consist of pure exponentials on the diagonal.

Using this result, the solution to Eq. (2.14) can be written as

$$x(t) = Me^{Jt}M^{-1}x(0). \tag{2.17}$$

This can further be decomposed if one considers the generalized modes of the system. A generalized mode in this context is meant as the solution to the ODE, with an initial condition in a linear combination of vectors in *one* of the Jordan chains. It can be shown that the trajectory then never leaves that Jordan chain throughout the whole evolution.

To show this, suppose first that the initial state is in such an initial state, i.e., in a linear combination of vectors in one of the Jordan chains:

$$x(0) = a_1 r_i + a_2 r_i^{(2)} + \dots + a_{n_i} r_i^{(n_i)} = \boldsymbol{r}_i a, \tag{2.18}$$

where $a = (a_1, \dots a_{n_i})^T$ is a constant vector and $\boldsymbol{r}_i$ is defined in Eq. (2.11). Inserting this into Eq. (2.17), the solution can be written as

$$x(t) = Me^{Jt}M^{-1}x(0) = Me^{Jt} \begin{bmatrix} \boldsymbol{l}_1 \\ \vdots \\ \boldsymbol{l}_q \end{bmatrix} \boldsymbol{r}_i a = \boldsymbol{r}_i e^{J_{n_i}(\lambda_i)t} a. \tag{2.19}$$

Hence, the solution stays in the space spanned by the initial condition throughout the evolution, as earlier proposed. For an arbitrary initial condition, the solution can be written as a sum over these generalized modes:

$$x(t) = \sum_{i=1}^{q} \boldsymbol{r}_i e^{J_{n_i}(\lambda_i)t} \boldsymbol{l}_i x(0), \tag{2.20}$$

and the initial condition therefore decides what modes are included in the dynamics of the system.

Translating this theory into the language of Liouvillian physics, the underlying ODE is given by the Lindblad equation, transformed to Fock-Liouville space

$$\frac{\mathrm{d}\rho(t)}{\mathrm{d}t} = \mathcal{L}\rho(t) \to \frac{\mathrm{d}}{\mathrm{d}t} |\rho(t)\rangle\rangle = L |\rho(t)\rangle\rangle, \tag{2.21}$$

where $L$ is the matrix representation of the Liouvillian and $|\rho(t)\rangle\rangle$ the vectorized density matrix. Using Eq. (2.20), the solution can then be written in terms of the eigenvalues and generalized eigenvectors of $L$.

# Chapter 3

# The system

In this thesis, a particular quantum dot system was studied, consisting of two quantum dots connected to two leads in thermal equilibrium. The quantum dots are assumed to be coupled in parallel to the leads, meaning that the dots are coupled to the same lead on each side. Furthermore, it is assumed that there is no direct tunneling between the dots, however with a non-zero Coulomb interaction between the dots if they are both occupied. A sketch of the model is given in Fig. 3.1.

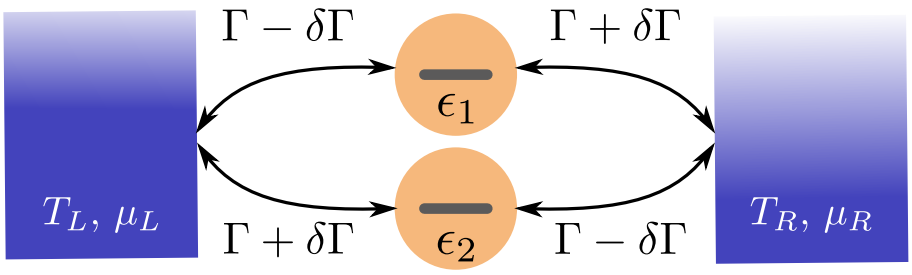


Figure 3.1: The modeled parallel dot system, where the quantum dots in the center have energies $\epsilon_1$ and $\epsilon_2$. Located on the sides are the two reservoirs $R, L$ with temperatures $T_{L/R}$ and chemical potentials $\mu_{L/R}$. The allowed tunneling processes are indicated with arrows, with corresponding tunneling rates $\Gamma \pm \delta\Gamma$.

To reduce the dimension of the parameter space, a fixed tunneling rate $\Gamma$ and a variable tunneling detuning $\delta\Gamma$ are introduced. The four tunneling rates in terms of $\Gamma$ and $\delta\Gamma$ are assumed to be asymmetric, as indicated by Fig. 3.1. It is also assumed that each dot is restricted to be either empty or contain one (spinless) electron in the ground state of the dot. The energy of the ground state $\epsilon_{1/2} = -V_{\mathrm{G}} \pm \delta\epsilon$ is given in terms of a fixed gate voltage $V_{\mathrm{G}} = 0$ and a variable energy detuning $\delta\epsilon$. Furthermore, the temperatures of the leads $T_{\mathrm{L}} = T_{\mathrm{R}} = 10\Gamma$, the chemical potentials $\mu_{\mathrm{L/R}} = \pm V_{\mathrm{SD}}/2$, the bias voltage $V_{\mathrm{SD}} = 300\Gamma$, and the Coulomb energy $U = 250\Gamma$, are all fixed in terms of $\Gamma$. This leaves the two tuning parameters, $\delta\Gamma$ and $\delta\epsilon$, as the only parameters of the system, resulting in a two dimensional parameter space.

The Hamiltonian of the total system can be modeled by $\hat{H} = \hat{H}_{\mathrm{QD}} + \hat{H}_{\mathrm{leads}} + \hat{H}_{\mathrm{tunneling}}$, where the three terms correspond to the quantum dot, lead, and tunneling

Hamiltonians:

$$\begin{aligned}\hat{H}_{\text{QD}} &= \sum_{i=1,2} \epsilon_i \hat{d}_i^\dagger \hat{d}_i + U \hat{d}_1^\dagger \hat{d}_1 \hat{d}_2^\dagger \hat{d}_2, \\ \hat{H}_{\text{leads}} &= \sum_{k,s=\text{L,R}} E_{s,k} \hat{c}_{s,k}^\dagger \hat{c}_{s,k}, \\ \hat{H}_{\text{tunneling}} &= \sum_{i=1,2} \sum_{k,s=\text{L,R}} t_{s,i} \hat{c}_{s,k}^\dagger \hat{d}_i + t_{s,i}^* \hat{d}_i^\dagger \hat{c}_{s,k},\end{aligned} \tag{3.1}$$

where $\hat{d}_i^\dagger$, $i \in \{1, 2\}$, creates an electron in dot 1 or 2, and $\hat{c}_{l,k}^\dagger$, $s \in \{\text{L,R}\}$, creates an electron in the left (L) or right (R) lead with momentum $k$ and energy $E_{s,k}$ [17]. The tunneling amplitudes $t_{s,i}$ can be approximated to be energy independent and are directly related to the corresponding tunneling rates by

$$\Gamma_{s,i} = 2\pi\nu_F |t_{s,i}|^2, \tag{3.2}$$

where $\nu_F$ is the density of states in the lead [14].

To represent the operators in matrix form, the many-body eigenstates of the isolated quantum dot Hamiltonian are used as the basis:

$$\begin{aligned}|a\rangle &= |00\rangle \\ |b\rangle &= |10\rangle = \hat{d}_1^\dagger |00\rangle \\ |c\rangle &= |01\rangle = \hat{d}_2^\dagger |00\rangle \\ |d\rangle &= |11\rangle = \hat{d}_1^\dagger \hat{d}_2^\dagger |00\rangle ,\end{aligned} \tag{3.3}$$

where $n_1$ and $n_2$ in $|n_1 n_2\rangle$ are the number of electrons in dot first and second quantum dot, respectively. The quantum dot and tunneling Hamiltonians are in this basis given by

$$\begin{aligned}\hat{H}_{\text{QD}} &= \epsilon_1 |b\rangle\langle b| + \epsilon_2 |c\rangle\langle c| + (\epsilon_1 + \epsilon_2 + U) |d\rangle\langle d| \\ \hat{H}_{\text{tunneling}} &= \sum_{k,s=\text{L,R}} \left[ t_{s,1}^* (|b\rangle\langle a| + |d\rangle\langle c|) + t_{s,2}^* (|c\rangle\langle a| - |d\rangle\langle b|) \right] \hat{c}_{s,k} + \text{H.c.}\end{aligned} \tag{3.4}$$

In the basis given by Eq. (3.3), the elements of the reduced density matrix can be written as $\rho_{\alpha\beta}$, where $\alpha, \beta \in \{a, b, c, d\}$, with 16 matrix elements. However, the only non-zero off-diagonal elements are $\rho_{bc}$ and $\rho_{cb}$, i.e, the elements which corresponds to superpositions the two states with one occupied dot. This is the result of charge being a conserved quantity in the total system (source?). The number of elements in $|\rho\rangle\rangle$ is therefore reduced to 6, which in turn means that the Liouvillian effectively can be represented by a $6 \times 6$ matrix.

To be able to justify the Lindblad approach for calculating the dynamics of the system, one more major approximation have to be made regarding the coupling between the dots and the leads. We must assume that the strength of the coupling between the system and the environment is weak in comparison with the other energy scales in the system, i.e., $\Gamma \ll T, U$. In this limit, the Lindblad equation is a standard approach for investigating the dynamics of a quantum dot system.

# Chapter 4

# Results

The first step towards simulating the dynamics of the parallel quantum dot system was to calculate the matrix representation of the Liouvillian. This was done numerically using an already implemented PERLind approach to calculate the four jump operators $\hat{L}_i$, $i \in \{1, 2, 3, 4\}$, each associated with one of the tunneling processes of the system (should I explain which jump operator corresponds with what tunneling process?). The total Liouvillian could then be constructed and compared with the Python-based QmeQ package ([18]) as a sanity check. Then, the parameter space was searched for exceptional points by numerically calculating the eigenvalues of $L$ for varying $\delta\epsilon$ and $\delta\Gamma$. A degeneracy of eigenvalues was found at $\lambda_5 = \lambda_6 \approx -0.5\Gamma$, for $\delta\Gamma = 10^{-6}\Gamma$ and $\delta\epsilon \approx 0.3\Gamma$, see Fig. 4.1. The corresponding eigenvectors, $|\rho_5\rangle\rangle$ and $|\rho_6\rangle\rangle$, was found to also coalesce, confirming the existence of an exceptional point. The eigenvalue and the left and right eigenvector corresponding to the EP will be denoted by $\bar{\lambda}$, $\langle\langle\bar{\sigma}|$, and $|\bar{\rho}\rangle\rangle$ respectively.

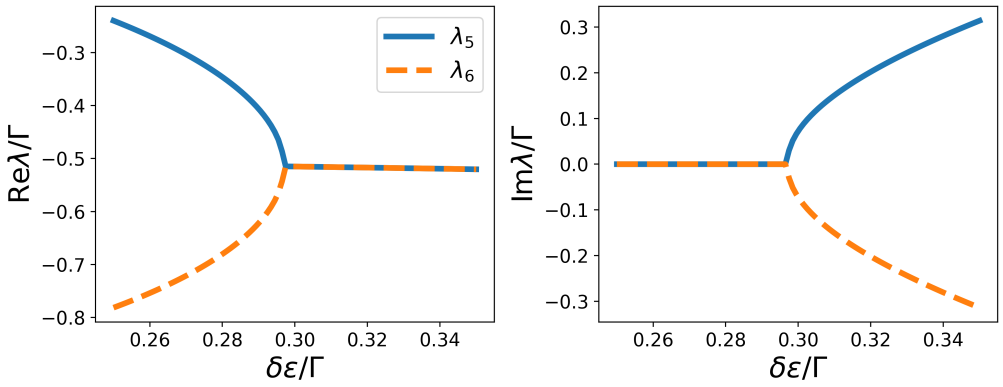


Figure 4.1: The real and imaginary part of two eigenvalues to $L$, $\lambda_5$ and $\lambda_6$, for varying $\delta\epsilon$. An eigenvalue degeneracy at can be seen at $\delta\epsilon \approx 0.3\Gamma$.

The full spectrum of the Liouvillian at the exceptional point is given in Fig. 4.2, where the eigenvalue degeneracy between $\lambda_5$ and $\lambda_6$ is clear. There is almost a degeneracy between $\lambda_3$ and $\lambda_4$, however, this is not a second EP since the eigenvectors are not parallel. Furthermore, note that all eigenvalues are on the negative real axis, indicating exponential decay towards the steady-state in the dynamics of the system.

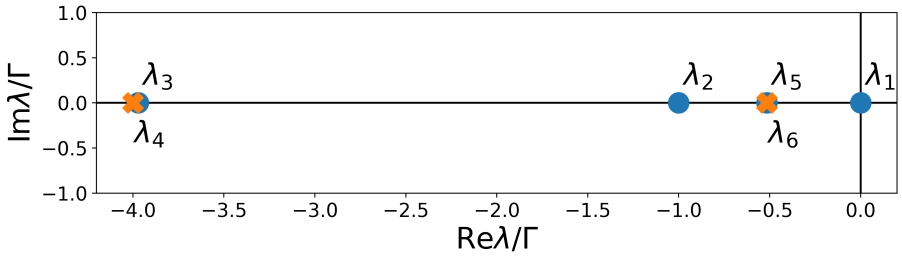


Figure 4.2: The spectrum of the Liouvillian at the exceptional point. The crosses are used to distinguish eigenvalues which are close to each other.

Using Eq. (2.20), the evolution of the system can be given in terms of the eigenvalues and generalized eigenvectors of $L$. Away from an exceptional point, the Liouvillian is diagonalizable, and the terms are purely exponential. The evolution of the density operator is then given by

$$|\rho(t)\rangle\rangle = |\rho_{ss}\rangle\rangle + \sum_{i=2}^{6} c_i e^{\lambda_i t} |\rho_i\rangle\rangle \tag{4.1}$$

where $|\rho_i\rangle\rangle$ is the $i$th right eigenvector of $L$, and $c_i = \langle\langle\sigma_i|\rho(0)\rangle\rangle$. Here, $\langle\langle\sigma_i|$ is the $i$th left eigenvector, constructed biorthogonally to $|\rho_i\rangle\rangle$. Furthermore, $|\rho_{ss}\rangle\rangle = c_1 |\rho_1\rangle\rangle$ is the steady state of the system, due to the zero eigenvalue $\lambda_1 = 0$.

At the exceptional point, the Jordan form of $L$ and its exponential $e^{Jt}$ have to be evaluated. Since the EP is of order two, this results in a $2 \times 2$ Jordan block. This is the only EP, which means that rest of the Jordan form is diagonal. Using Eqs. (2.13) and (2.16), this results in the following Jordan form and Jordan exponential:

$$J = \begin{bmatrix} 0 & 0 & 0 & 0 & 0 & 0 \\ 0 & \lambda_2 & 0 & 0 & 0 & 0 \\ 0 & 0 & \lambda_3 & 0 & 0 & 0 \\ 0 & 0 & 0 & \lambda_4 & 0 & 0 \\ 0 & 0 & 0 & 0 & \bar{\lambda} & 1 \\ 0 & 0 & 0 & 0 & 0 & \bar{\lambda} \end{bmatrix}, \quad e^{Jt} = \begin{bmatrix} 1 & 0 & 0 & 0 & 0 & 0 \\ 0 & e^{\lambda_2 t} & 0 & 0 & 0 & 0 \\ 0 & 0 & e^{\lambda_3 t} & 0 & 0 & 0 \\ 0 & 0 & 0 & e^{\lambda_4 t} & 0 & 0 \\ 0 & 0 & 0 & 0 & e^{\bar{\lambda} t} & t \\ 0 & 0 & 0 & 0 & 0 & e^{\bar{\lambda} t} \end{bmatrix}, \tag{4.2}$$

since $\lambda_1 = 0$.

Furthermore, the Jordan chain vector, here written as $|\rho'\rangle\rangle$, defined by $(L - \bar{\lambda} I)\,|\rho'\rangle\rangle = |\bar{\rho}\rangle\rangle$ and the corresponding left generalized eigenvector $\langle\langle\sigma'|$, need to be evaluated. Inserting these vectors into Eq. (2.20), the evolution of the density operator can be shown to be given by

$$|\rho(t)\rangle\rangle = |\rho_{ss}\rangle\rangle + \sum_{i=2}^{4} c_i e^{\lambda_i t} |\rho_i\rangle\rangle + (\bar{c} + c' t) e^{\bar{\lambda} t} |\bar{\rho}\rangle\rangle + c' e^{\bar{\lambda} t} |\rho'\rangle\rangle, \tag{4.3}$$

where $\bar{c} = \langle\langle\bar{\sigma}|\rho(0)\rangle\rangle$, and $c' = \langle\langle\sigma'|\rho(0)\rangle\rangle$.

By numerically calculating the generalized eigenvectors as described in section 2.3.1, the dynamics at non-EP and at EP given by Eqs. (4.1) and (4.3), could be implemented. The results were then compared with a numerical ODE-solver, see Fig. 4.3.

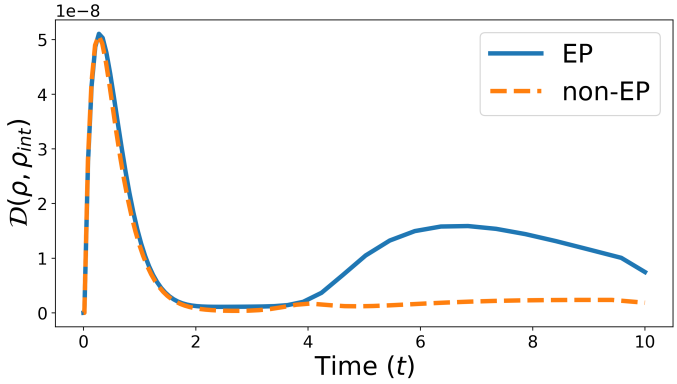


Figure 4.3: The relative distance $\mathcal{D}(|\rho\rangle\rangle, |\rho_{\text{int}}\rangle\rangle) = ||\,|\rho\rangle\rangle - |\rho_{\text{int}}\rangle\rangle||_1 / ||\,|\rho_{\text{int}}\rangle\rangle||_1$ between the density matrices calculated with the implemented methods and with a numerical solver. The two lines represent the distances at the EP and away from the EP, using the corresponding implemented methods for each case. The numerical solver was set to an absolute and relative tolerance of $10^{-10}$ and $10^{-6}$ respectively.

With a clear picture of the analytical dynamics and numerically calculated eigenvalues and generalized eigenvectors at hand, simulations of the parallel dot system could be done. Firstly, the evolution in the generalized modes was investigated. This was done by simulating the density matrix for initial conditions in terms of the generalized eigenvectors, and comparing it with the steady-state of the system, see Fig. 4.4a.

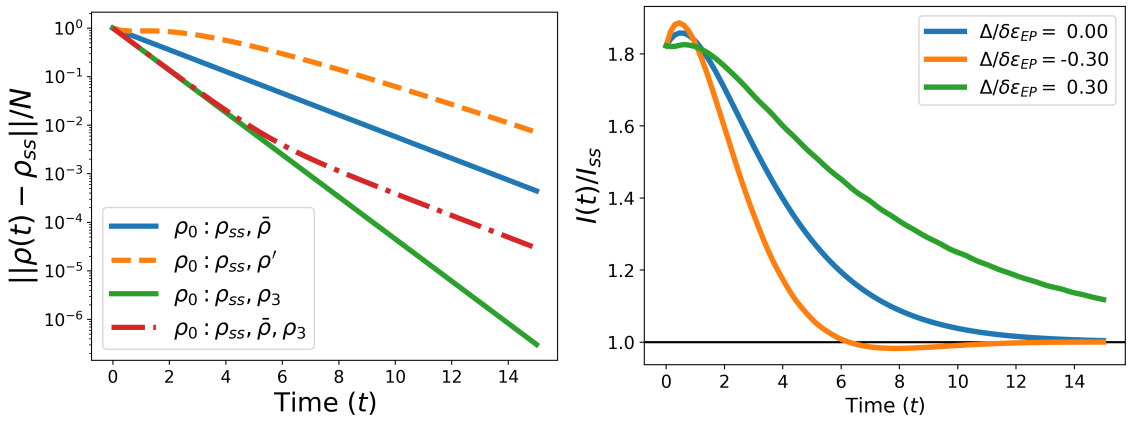


(a) (b)

Figure 4.4: a) The decay of the system towards the steady state $\rho_{ss}$ in a log plot. The simulations were done at the EP with different initial conditions. A normalization by $N = ||\rho(0) - \rho_{ss}||$ was done such that each curve is unity for $t = 0$. b) The current over time for different $\delta\epsilon$, normalized by the steady state current $I_{ss}$. The solid, blue curve correspond to the system being at the EP, while the other two are slightly away from it.

As discussed in the theory section, any relevant observable of the system can be obtained from the density operator. For the parallel dot system, the main observable is the current $\hat{I}$, which can be put in terms of the jump operators as follows:

$$\textit{something} \tag{4.4}$$

Using Eq. (2.3), the current could then be calculated with $\langle \hat{I} \rangle (t) = \mathrm{Tr}\,(\hat{\rho}(t)\hat{I})$. Implementing this numerically, the current through the quantum dot system for varying parameters and initial conditions could be simulated. In Fig. 4.4b, the dynamics of the current at and slightly away from the exceptional point was simulated.

Add more plots like this with different initial conditions?

# Chapter 5

# Discussion

From Fig. 4.3, it is clear that the implemented methods produce an accurate result at and away from the exceptional point. The relative distance to the numerical solver is on the order of $10^{-8}$, and with the use of strict tolerances of the numerical solver, this indicates an accurate method. Furthermore, when reducing the tolerances even more, the distance kept lowering, indicating that the numerical solver might be the limiting factor.

Using the calculated generalized eigenvectors, the evolution in the generalized modes given by Eq. (4.3), could be evidenced in **??**. With an initial condition only overlapping the steady state and one other normal eigenvector, a pure exponential decay toward the steady state is seen by the straight lines in the log plot. When including both $|\bar{\rho}\rangle\rangle$ and $|\rho_3\rangle\rangle$ in the initial condition, the decay first follows the quicker decay channel, then gradually turns into following the decay of $|\bar{\rho}\rangle\rangle$. Another behavior is seen for the initial condition including $|\rho'\rangle\rangle$. This decay channel is not of exponential nature, since a factor of $te^{\bar{\lambda}t}$ enters in the decay.

Something about the similarity of Fig. 4.4b to Haak's paper regarding critical damping.

The main takeaways from the implemented methods and the following simulations consist of two parts. Firstly, that the general evolution for the parallel quantum dot system at an EP indeed can be understood in terms of the sum of generalized modes given by Eq. (2.20). This means that the Jordan blocks evolve separately, and that the initial condition decides what modes are involved in the dynamics of the system. Secondly, that the implemented methods give direct access to the generalized eigenvectors through numerical means, which in theory can be done for even larger systems and higher order EPs, unlike algebraic methods. The generalized eigenvectors can then be used as initial conditions, directly controlling what Jordan blocks are included in the evolution.

Applications and further theoretical outlook?

# Bibliography


[1]Y. Ashida, Z. Gong, and M. Ueda, "Non-hermitian physics", Advances in Physics **69**, 249–435 (2020).

[2]H. Hodaei, A. Hassan, S. Wittek, H. Garcia-Gracia, R. El-Ganainy, D. Christodoulides, and M. Khajavikhan, "Enhanced sensitivity at higher-order exceptional points", Nature **548**, 187–191 (2017).

[3]W. Chen, Ş. Kaya Özdemir, G. Zhao, J. Wiersig, and L. Yang, "Exceptional points enhance sensing in an optical microcavity", Nature **548**, 192–196 (2017).

[4]S. Khandelwal, N. Brunner, and G. Haack, "Signatures of Liouvillian exceptional points in a quantum thermal machine", PRX Quantum **2**, 040346 (2021).

[5]P. Kumar, K. Snizhko, Y. Gefen, and B. Rosenow, "Optimized steering: quantum state engineering and exceptional points", Phys. Rev. A **105**, L010203 (2022).

[6]S. A. Gurvitz and Y. S. Prager, "Microscopic derivation of rate equations for quantum transport", Phys. Rev. B **53**, 15932–15943 (1996).

[7]L. Kouwenhoven and C. Marcus, "Quantum dots", Physics World **11**, 35–40 (1998).

[8]R. A. Bush, E. D. Ochoa, and J. K. Perron, "Transport through quantum dots: An introduction via master equation simulations", American Journal of Physics **89**, 300–306 (2021).

[9]Dorsch, Sven, "Transport in nanowire-based quantum dot systems: Heating electrons and confining holes", eng, PhD thesis (Lund University, 2022).

[10]D. Manzano, "A short introduction to the Lindblad master equation", AIP Advances **10**, 025106 (2020).

[11]G. Schaller, *Open quantum systems far from equilibrium*, Vol. 881, Lecture Notes in Physics (2014).

[12]A. Iserles, *A first course in the numerical analysis of differential equations* (Cambridge University Press, 2009).

[13]G. Lindblad, "On the generators of quantum dynamical semigroups", Communications in Mathematical Physics **48**, 119–130 (1976).

[14]G. Kiršanskas, M. Franckié, and A. Wacker, "Phenomenological position and energy resolving lindblad approach to quantum kinetics", Phys. Rev. B **97**, 035432 (2018).

[15]A. Holst and V. Ufnarovski, *Matrix theory* (Studentlitteratur, 2014).

[16]R. A. Horn and C. R. Johnson, *Matrix analysis* (Cambridge University Press, 1985).

[17]Z.-Z. Li and M. Leijnse, "Quantum interference in transport through almost symmetric double quantum dots", Phys. Rev. B **99**, 125406 (2019).

[18]G. Kiršanskas, J. N. Pedersen, O. Karlström, M. Leijnse, and A. Wacker, "QmeQ 1.0: an open-source Python package for calculations of transport through quantum dot devices", Computer Physics Communications **221**, 317–342 (2017).